Research Article

Technical and Financial Viability of a 1 MW CSP Power Plant with Organic Rankine Module: Case Study for a Northeastern Brazilian City

João G. M. S. Ponte[1], Paulo Alexandre Costa Rocha[2]

1. Technical University of Munich (TUM), Munich, Germany; 2. Universidade Federal do Ceará, Brazil

In this study, a 1 MWe parabolic trough concentrating solar power plant using an Organic Rankine Cycle to convert thermal power into electricity was simulated. The solar data used is from Fortaleza, the capital city of Ceara, a state in the northeast region of Brazil. The simulation was year-round and used hourly acquired data. Several different configurations, differing in the number of collectors and the size of thermal energy storage, were considered, and by the end of the study, according to the technical and financial results, one best configuration was defined. With a net annual energy generation of 4815.50 MWh, a 12.08% total efficiency, and a levelized cost of electricity (LCOE) of 186.98 US$/MWh, the best-defined configuration was the one with 100 collector assemblies and a 48 MWh storage system. Besides that, the capital and OM costs of the various components were compared to define the most expensive for the power plant, with the collectors' acquisition being the biggest cost, representing 74% and 58% of capital and OM costs, respectively.

Correspondence: papers@team.qeios.com — Qeios will forward to the authors

List of Abbreviations

- **HTF**: Heat Transfer Fluid
- **O&M**: Operation and Maintenance

Nomenclature

- Δh_{field}: HTF enthalpy change between the inlet and the outlet of the solar field $[J/kg]$
- ΔT: difference between the average temperature of the solar field and the ambient temperature $[^{\circ}C]$

 doi.org/10.32388/NKKKOI

- $\dot{W}_{pump}$: Power consumption of the pump $[W]$
- η_{field}: field efficiency that accounts for losses due to mirror optics and imperfections $[\%]$
- η_{HCE}: HCE efficiency that accounts for losses due to HCE optics and imperfections $[\%]$
- $\eta_{pumpref}$: reference HTF pump efficiency $[\%]$
- η_{pump}: HTF pump efficiency $[\%]$
- $\rho(T_1)$: HTF density evaluated at the solar field inlet temperature $[kg/m]$
- Θ: incidence angle $[deg]$
- a, b: coefficients available in tables 3 to 5 for different annulus vacuum conditions $[-]$
- $BelShad$: losses due to shading of ends of HCEs due to bellows $[-]$
- C_{fuel}: annual fuel costs (equals to 0, since it's a stand-alone solar plant) [$]
- C_{invest}: investment costs [$]
- $C_{\&M}$: annual operation and maintenance costs [$]
- $ColFrac$: fraction of collector type in the field $[-]$
- DNI: direct normal insolation $[W/m^2]$
- e_{mo}: factor for calculating the HTF pump efficiency (assumed 0.4) $[-]$
- $EndLoss$: performance factor that accounts for losses from ends of HCEs $[-]$
- $EnvTrans$: transmissivity of the glass envelope $[-]$
- f: focal length of the collectors (5 meters at SEGS VI) $[m]$
- fcr: annuity factor $[\%]$
- $GeoAcc$: geometric accuracy of the collector mirrors $[-]$
- $HCEabs$: absorptivity of the HCE selective coating $[-]$
- $HCEdust$: losses due to shading of HCE by dust on the envelope $[-]$
- $HCEEmisc$: miscellaneous factor to adjust for other HCE losses $[-]$
- $HCEFrac$: fraction of HCE type in the field $[-]$
- IAM: incidence angle modifier $[-]$
- K: constant for calculating the IAM $[-]$
- L_{SCA}: length of a single solar collector assembly (50 meters at SEGS VI) $[m]$
- $L_{spacing}$: distance between collector rows $[m]$
- $LCOE$: levelized cost of energy $[US\$/MWh]$
- m_{HTFref}: reference HTF mass flow $[kg/m^3]$
- m_{HTF} HTF mass flow $[kg/m^3]$
- $MirCln$ mirror cleanliness $[-]$
- $MirRef$ mirror reflectivity $[-]$

- n number of periods (assumed as 30 years of operation) $[years]$
- N_{SCA} number of collector assemblies in the solar field $[-]$
- $NumCol$ the number of collector types in the field $[-]$
- $NumHCE$ number of HCE types in the field $[-]$
- Q_{abs} radiation absorbed by the HCE $[W/m^2]$
- $Q_{collected}$ energy collected by the solar field $[W/m^2]$
- r loan rate (assumed 7% according to [1]) $[\%p.a.]$
- $RowShadow$ performance factor which accounts for the mutual shading of parallel collector rows during early morning and late evening $[-]$
- $SFAvail$ fraction of the solar field that is operable and tracking the sun $[-]$
- T bulk fluid temperature $[^\circ C]$
- T_0 temperature in the solar field outlet $[^\circ C]$
- T_1 temperature in the solar field inlet $[^\circ C]$
- $TrkWstErr$ twisting and tracking error associated with the collector type $[-]$
- V_{HTF} volumetric flow rate of the HTF entering the solar field $[m^3/s]$
- W collector wideness $[m]$
- W_{eff} effective collector wideness $[m]$

1. Introduction

In today's context, renewable energy sources are playing a bigger role in electricity generation than years ago. Between 2016 and 2017, the world saw an increase of 178 GW in renewable generation installed capacity, a rise of 8.82%. In a somewhat different way, concentrating solar power is still growing at a slow pace, 0.1 GW from 2016 to 2017, reaching 4.9 GW, which represents only 0.22% of the total renewable capacity in that year [2]. Even though the investments in CSP are still low when compared to wind and photovoltaics, it is still one of the most promising technologies to help in the transition from traditional thermal generation to renewables, mostly due to the possibility of decoupling energy production from the solar source with the use of an energy storage system [3]. Concentrating solar power consists of harvesting the energy from the Sun's radiation in the form of heat for electrical power production by concentrating the direct solar radiation onto a receiver and using a heat engine for power conversion. In order to do that, a set of different thermal cycles may be implemented, such as Rankine or Stirling [4]. Typically, for parabolic trough collectors, the Rankine cycle is implemented [4] and it should be used as a baseline comparison for the present paper. The main features that a site must have to be suitable for such a power plant are abundant direct sunlight (DNI, direct normal irradiation) during most of the year and high average temperatures to reduce heat losses to the ambient. Solar power is inherently

intermittent, and due to that, CSP can be implemented together with a thermal energy storage (TES) solution, a system responsible for storing the excess thermal energy production during peak hours and using it during cloudy or night hours. The TES allows the CSP power plant to have greater efficiency and availability [5]. Although this technology has been the topic of studies for several years [6], it still is a field presenting continuous developments, as investigated by [7] who analyses the present status and the development tendency of CSP, and being the focus of many recent researches which address many issues related to it. In [8], a fully renewable system comprising wind, CSP, and biomass power plants, and pumped-storage facilities was analysed. The authors presented CSP as crucial for the operation of such a system, due to the fact that plants with TES are dispatchable and can adjust their production to the demand, providing more flexibility to the system. [9] investigates the feasibility of CSP in Sub-Saharan Africa and concludes, among other things, that the financing conditions are the most important factor to determine the CSP feasibility for that region. In [10], the economic justification of CSP was analysed when taking into account not only the selling price of energy but also the flexibility provided to the system and the economic gain due to it in two provincial power systems with high renewable penetration in northwestern China. Conclusions could be drawn, such as that CSP investment is more cost-efficient in systems with deficient operational flexibility, and that substituting variable renewable energy with CSP brings considerable reductions in thermal generation fuel costs, ramping costs, and start-stop costs, in which the fuel cost reductions are the dominant contributor. When it comes to Brazil, the CSP technology still must carve its way inside the country's energy matrix, since in the past decades all the investments in renewable capacity went to hydro, wind, PV, or biomass generation [11]. Being near the Equator line, Brazil's northeastern region presents good potential for CSP projects, with an average DNI reaching around 5500 Wh/m^2. day and average annual temperatures above 24°C [12]. Furthermore, the region has seen a great rise in wind and solar power generation [11], which brings instability to the system and makes CSP projects more attractive for the system operator in order to compensate for the typical PV and wind variations with a dispatchable and stable renewable capacity [10]. This rise can be seen in Figure 1, where the power generation by source of the region is shown for the period from 2010 until 2018.

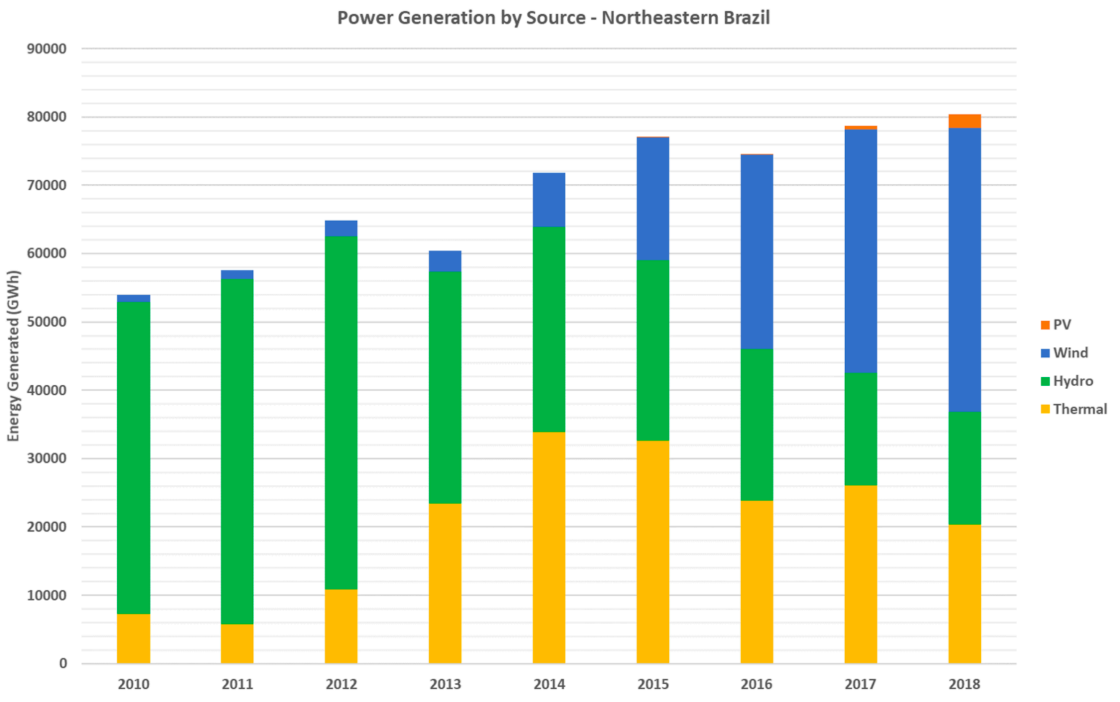

Figure 1. Annual power generation by source for the Northeastern region of Brazil between 2010 and 2018 [11]

Taking these local favourable conditions into account, in this paper, a 1 MWe CSP power plant with an Organic Rankine Cycle (ORC) power block is proposed, and the technical and economic results of a year-round operation are estimated, analysed, and compared with values of Levelized Cost of Electricity (LCOE) presented as a trend in [2] and with the results obtained in [1] for a hybrid CSP and biomass power plant also in the northeastern region of Brazil. In order to do so, several configurations were considered, differing from one another in the solar field size and in the implementation or not of a TES and the amount of its storage capacity. The LCOE was calculated for a 30-year operating period, and the optimum configuration was chosen based on the lowest result. The present work utilizes local sunlight data from a Brazilian northeastern city for the calculations, thus reaching results that should approximate the reality of this region, which doesn't have any working plant of the kind in its territory, despite the good potential it presents. This has been investigated also by [1], where a hybrid CSP and biomass power plant is simulated for a region of the state of Bahia in the northeastern region of Brazil. Furthermore, this study raised the Organic Rankine Cycle (ORC) technology as a suitable option to allow a relatively efficient operation at lower temperatures and for a small capacity, as was done in [13], where a model to analyze the impact of different design parameters on the LCOE of a 1MWe plant is proposed. The ORC application for such a power plant was also analysed by [14], although for smaller systems (up to 50kW). The technology chosen for the solar field was the parabolic trough collectors (PTCs), as it is the most commercially

available and tested among the thermal collector options, presenting higher efficiency than the solar tower and Fresnel technologies [4][15]. The novelty of the present work relies on many of its aspects. At first, the chosen location, a Brazilian northeastern city, has not been studied for this kind of undertaking, even though it presents two important aspects to attract investments in the field: the region has favourable weather conditions for the presented technology, and it has a large population, causing it to be a high-demand location for the transmission system. Together with the mentioned aspects, the Brazilian integrated system already faces a challenge that should only increase in the years to come: the instability brought to the grid by renewable capacity from wind and solar, causing this kind of investment to be even more attractive for the operator. Given all that, sunlight data measured in the city of Fortaleza was applied in the calculations performed here. Another novel aspect of this study is the utilization of a real commercially available ORC module for the power conversion with the goal of allowing the implementation of a small-capacity power plant ($1MWe$) but with high flexibility and low maintenance costs. This can be a good alternative for a first investment of the kind in the region, since the discussion is centered on a region that has no precedent in the CSP business. The third novelty presented here is the sizing of the solar field as a function of the chosen ORC module in order to obtain the best configuration for the plant regarding solar field size and storage capacity, with the goal of obtaining the lowest LCOE possible given the chosen constraints. Through the economic analysis, it was possible to state the components that influence the obtained energy price the most and to understand how the storage capacity and the solar multiple affect the LCOE of each configuration. This paper should foster discussions and further studies for the region regarding this kind of technology in order to develop a scenario more prone to receive investments from companies and institutions interested in further developing the renewable energy sector in Brazil and, more specifically, its northeastern region. Currently, this region doesn't have a wide enough background to rely on or to draw the interest of such players. In section 2 of this work, the system modeling is described for each of its components with all the physical and empirical equations used and the assumptions made. Section 3 is used to present the parameters considered for the economic analysis of the power plant and how the LCOE was calculated. An overview of the simulation is given using an hourly operation graph for one day and a Sankey diagram for one specific hour of the day. In section 5, the results are presented and discussed, and the final conclusions are drawn in section 6.

2. System Modeling

The model was applied utilizing Sun irradiation data acquired at the airport of Fortaleza city (3° 46′ 33″ S 38° 31′ 56″ W), the capital of Ceara, a northeastern state of Brazil. The data provide hourly values for Direct Normal Irradiation (DNI) throughout a year and are available as weather data from the software System Advisor Model by the National Renewable Energy Laboratory (NREL) [16], which acquires those values through ground

measurements, satellite data, or both. The solar field model was based on [17] and [6], where all the equations needed to calculate the necessary angles and the thermodynamic performance of the solar field were taken from. The collector considered was the LUZ LS-2, the same model implemented in some of the SEGS power plants in the Mojave Desert in California [6]. The option for this collector model enables better comparison possibilities between the results obtained and the vast amount of data and studies based on the SEGS power plants. In the next subsections, the mathematical description of the different subsystems is described. Subsections 2.1, 2.2, and 2.3 present the equations and assumptions used for the power block, the solar field, and the thermal storage system, respectively, and subsection 2.4 describes the different configurations considered in this paper.

2.1. Power Block

The main constraint of the system is the ORC module, since it defines the amount of power being generated according to the thermal energy supplied at the evaporator and the temperature at which this energy is supplied, thus regulating the energy transferred to and from the TES. The module considered in this paper is the same for all the 10 configurations and generates a net electric energy of 964 kW with 4043 kW of thermal energy from the HTF, reaching a 23.8% net efficiency at base load [18]. For operation under base load conditions, a linear drop of 1% in efficiency for every 5% in load was considered, according to the efficiency curve presented in [18]. Table 1 summarizes the main technical data of the ORC module.

INPUT – Thermal Oil	
Nominal Temperature (in/out)	**Thermal Power Input**
305/209°C	4043kW
OUTPUT – Cooling Water	
Cooling Water Temperature (in/out)	**Thermal Power to the Cooling Water Circuit**
25/35°C	3040kW
PERFORMANCES	
Gross Electric Power	**Gross Electric Efficiency**
1000kW	24.7%
Net Active Electric Power Output	**Net Electric Efficiency**
964kW	23.8%

Table 1. Typical operational values for energy input and output and general performance of the ORC module TURBODEN [18] 12 HRS - 1MW without split provided by the manufacturer.

As can be found in the literature [17] [19], the percentage of the gross power production that is consumed by the cooling water pumping system lies around 2.26%. Given that, a percentage of 2.5% was used as a reasonable

assumption for the present work. The variation of ambient conditions was not considered to cause a greater impact on the operation of the cooling system, being thus neglected.

2.2. The Solar Collectors Field

Before any mathematical modelling, it's important to determine the design point for the given solar power plant. Usually, the design point irradiation is taken at the equinox at 10 am [20]. For 2019, the equinox was on the 23rd of September, so the design point for the present paper will be considered on that date at 10 am. Starting with the absorbed radiation equation, the solar field model determines how much energy the collectors are harvesting from the Sun. Equation 1 calculates the absorbed energy as a function of the Direct Normal Insolation (DNI) and many other factors that tend to lower the fraction that is really absorbed:

$$Q_{abs} = DNI \cdot cos(\theta) \cdot IAM \cdot RowShadow \cdot EndLoss \cdot \eta_{field} \cdot \eta_{HCE} \cdot SFAvail \tag{1}$$

Each of the factors presented in the equation is discussed separately in sections 2.2.1 until 2.2.4, and the necessary equations for estimating them are presented. All these equations were taken from the literature [17]. Heat losses are modelled in subsections 2.2.5 and 2.2.6, the energy gain equation for the HTF is presented in 2.2.7, and sections 2.2.8 and 2.2.9 address the power consumption of the HTF circulating pumps and how the HTF flow rate control is carried out, respectively.

2.2.1. Incidence Angle Modifier (IAM)

The incidence angle not only influences the absorbed radiation through the cosine present in the equation but also through other losses that must be considered. They occur due to additional reflections and absorptions by the mirrors as a result of the increment in the incidence angle. The model assumed for these losses results from empirical data of the LS-2 collectors and is formulated according to equations 2 and 3.

$$K = cos(\theta) + 0.000884(\theta) - 0.00005369(\theta)^2 \tag{2}$$

$$IAM = \frac{K}{cos(\theta)} \tag{3}$$

2.2.2. Shading

The shading due to parallel adjacent collector rows occurs in the early hours of the day and late hours of the afternoon, and it is estimated by equation 4. The effective wideness is the portion of the aperture that receives sunlight, which means it is not covered by shadow.

$$RowShadow = \frac{W_{eff}}{W} = \frac{L_{spacing}}{W} \cdot \frac{cos(\theta_z)}{cos(\theta)} \tag{4}$$

2.2.3. Heat Collecting Element (HCE) End Losses

The end of the HCE is responsible for a heat loss, since, depending on the incidence angle, a portion of the element won't receive radiation due to the collector structure. Equation 5 estimates a value for that factor:

$$EndLoss = 1 - \frac{f \cdot tan(\theta)}{L_{SCA}} \tag{5}$$

2.2.4. Solar Field and HCE Efficiencies

The last factors to be considered account for mirror imperfections, dirtiness, reflectivity of the HCE glass, among others. They are modelled by equations 6 and 7:

$$\eta_{field} = \sum_{i=1}^{NumCol} ColFrac_i \cdot TrkTwstErr_i \cdot GeoCac_i \cdot MirRef_i \cdot MirCln_i \tag{6}$$

$$\eta_{HCE} = \sum_{i=1}^{NumHCE} HCEfrac_i HCEdust_i \cdot BelShad_i \cdot EnvTrans_i \cdot HCEabs_i \cdot HCEmisc_i \tag{7}$$

Name	Value	Name	Value
TrkTwstErr	0.99	HCEdust	0.98
GeoAcc	0.98	BelShad	0.97
MirRef	0.93	EnvTrans	0.96
MirCln	0.95	HCEabs	0.95
		HCEmisc	0.96

Table 2. Typical optical parameters and correction values for the solar field and HCE efficiencies [17].

2.2.5. Heat Collector Element (HCE) Heat Losses

For the HCE heat losses, the model developed by [21] and utilized in [17] was also implemented in the present work. Many factors like wind speed, incident radiation, HTF mass flow rate, ambient temperature, and bulk fluid temperature can have an influence on the heat lost to the surroundings, but to make a simpler model and optimize the computational overhead, the DNI and the fluid temperature were considered as the main influencing factors. With these assumptions and through a linear regression of the calculated heat loss per unit length over a range of bulk fluid temperatures and DNI levels, for a UVAC tube with a cermet selective coating, at an ambient temperature of 25 $^{\circ}C$ with a volumetric flow rate through each collector of 140 gal/min the equation 8 is obtained.

$$HeatLoss = a_0 + a_1 \cdot T + a_2 \cdot T^2 + a_3 \cdot T^3 + DNI \cdot (b_0 + b_1 \cdot T^2) \tag{8}$$

Parameter	Value	Standard Deviation
a0	-9.463033E+00	8.463850E-01
a1	3.029616E-01	1.454877E-02
a2	6.929243E-06	7.305717E-05
a3	6.929243E-06	1.070953E-07
b0	7.649610E-02	5.293835E-04
b1	1.128818E-07	6.394787E-09
RMS	**2.4 [W/m]**	

Table 3. Coefficients for the Receiver Heat Loss: Vacuum Annulus

Parameter	Value	Standard Deviation
a0	-2.247372E+01	1.399498E+00
a1	8.374490E-01	8.335284E-03
a2	0.00	———
a3	4.620143E-06	4.538542E-08
b0	6.983190E-02	1.550570E-03
b1	9.312703E-08	1.872309E-08
RMS	**8.1 [W/m]**	

Table 4. Coefficients for the Receiver Heat Loss: Air Annulus

Parameter	Value	Standard Deviation
a0	-3.583342E+01	3.895262E+00
a1	1.461366E+0	6.695686E-02
a2	1.569955E-03	3.362262E-04
a3	4.013432E-06	4.928776E-07
b0	6.926351E-02	2.436347E-03
b1	1.382089E-07	2.943031E-08
RMS	**12.7 [W/m]**	

Table 5. Coefficients for the Receiver Heat Loss: Hydrogen Annulus

Since the temperature varies along the HCE, the equation has to be integrated for the inlet and outlet temperatures. In addition, the result should be divided by the collector aperture in order to represent the heat loss in W/m^2. Equation 9 is obtained, and it is utilized for a single type of HCE and with optimum vacuum conditions.

$$HL_{field} = \frac{a_0 \cdot (T_0 - T_1) + \frac{a_1}{2} \cdot (T_0^2 - T_1^2) + \frac{a_2}{3} \cdot (T_0^3 - T_1^3) + \frac{a_3}{4} \cdot (T_0^4 - T_1^4)}{(T_0 - T_1) \cdot W} + \frac{DNI \cdot (b_0 \cdot (T_0 - T_1) + \frac{b_1}{3} \cdot (T_0^3 - T_1^3))}{(T_0 - T_1) \cdot W} \quad (9)$$

2.2.6. Piping Heat Losses

The heat losses of the solar field piping system can be estimated by the empirical equation 10 :

$$SfPipeHl = 0.01693 \cdot \Delta T - 0.0001683.\Delta T^2 + 6.78 \cdot 10^{-7} \cdot \Delta T^3 \quad (10)$$

where SfPipeHl is expressed in W/m^2 and ΔT is the difference between the average temperature of the solar field and the ambient temperature. Generally, the piping losses are small, reaching values around 10 W/m^2 or less during operation [17].

2.2.7. HTF Energy Gain and Temperature Rise

The energy collected by the solar field is the difference between the heat absorbed and the heat losses presented previously.

$$Q_{collected} = Q_{absorbed} - (RecHl + SfPipeHl) \quad (11)$$

The solar field was assumed to operate at steady-state conditions, and the kinetic and potential energy changes were neglected. The enthalpy variation of the HTF is then calculated by equation 12:

$$\Delta h_{field} = \frac{Q_{collected} \cdot W \cdot L_{SCA} \cdot N_{SCA}}{V_{HTF} \cdot \rho(T_1)} \quad (12)$$

The density of Therminol VP-1 as a function of its temperature is represented by equation 13 [17]:

$$\rho(T) = 1074 - 0.6367 \cdot T - 0.0007762 \cdot T^2 \quad (13)$$

And the temperature and specific enthalpy as functions of one another are represented by equations 14 and 15 [17]:

$$h(T) = 1000 \cdot (-18.34 + 1.498 \cdot T + 0.001377 \cdot T^2) \quad (14)$$

$$T(h) = -1.58E(-10) \cdot h^2 + 0.0006072 \cdot h + 13.37 \quad (15)$$

2.2.8. HTF Pump Power Consumption

The power consumption of the HTF pump was calculated using [17] as a reference. In that work, the author had the pump rated power as input and calculated the pressure drop with equation 16

$$\Delta P = \frac{\eta_{pump} \cdot W_{pump}}{V_{HTF}} \quad (16)$$

Here, the inverse path was made, considering the pressure drop as proportional to the number of collectors in the field. Given that, the power consumed was calculated with the pressure drop, the efficiency of the pump, and the volumetric flow as inputs. In addition, the efficiency of the pump was considered to be 60% at nominal operation, as in [17], which would be for the 23rd of September at 10 am, according to the design point stated at the beginning of section 2.2, and it was corrected with the flow variation according to equation 17.

$$\frac{\eta_{HTF}}{\eta_{HTFr}} = e_{mo} + 2(1 - e_{mo})(\frac{m_{HTF}}{m_{HTFr}}) - (1 - e_{mo})(\frac{m_{HTF}}{m_{HTFr}})^2 \quad (17)$$

2.2.9. Heat Transfer Fluid (HTF) Flow Rate and Outlet Temperature Control

During night or cloudy hours, keeping the HTF circulating would result in heat losses without any gain. Given that, it was assumed that the pumps would feed the solar field with HTF only if the absorbed heat surpasses the 75 W/m^2 threshold. Furthermore, the ORC module is specified for a certain temperature for the oil entering the evaporator. In order to meet such a constraint, the outlet temperature of the solar field was specified at 310°C under normal operation, and the HTF flow rate keeps changing in order to control that temperature; that is, the volumetric flow rate may increase during higher insolation times.

2.3. Thermal Energy Storage (TES)

Since the heat losses for the HTF were accounted for in the solar field, heat losses associated with TES were considered to be too small (0 kW/K as in [17]. All the excess thermal energy collected by the solar field is stored in the hot tank (until it reaches its peak storage capacity), and as long as it still has energy stored inside of it, the TES will keep supplying thermal energy to the power block.

2.4. Considered Configurations

For this study, all the configurations considered have the same power block specified in Section 2.1. These differed regarding the presence or absence of TES storage capacity. Five different solar field sizes were also considered: 50, 75, 100, 125, and 150 PTC assemblies. With the chosen design point stated at 2.2 as a reference with a DNI of 810 W/m^2, the Solar Multiple (SM) of these solar field sizes are 1.42, 2.13, 2.85, 3.56, and 4.27. The optimum configuration from those was defined based on the economic analysis, which is presented and explained further on.

3. Economic Analysis

In order to define the financial parameters of the power plant, the different components (solar field, TES, power block) are analyzed separately. Typical values found in the literature are considered for both the acquisition and

OM costs of the components mentioned. These values are applied for the calculation of the Levelized Cost Of Electricity (LCOE).

3.1. Solar Field Costs

Based on the literature [22], the acquisition cost of the collectors usually lies between 150-200 $\$/m^2$. In addition to that, an annual maintenance cost of 3.72 $\$/m^2$ is considered [23].

3.2. TES Costs

The values for the cost calculations of the TES are based on a molten salt configuration, which can be justified by the solidification temperature of 142 $^\circ$ presented in [24] for a mixture of $NaNO_2/KNO_3/NaNO_3$. The literature studied proposes a usual capital cost of 26.22 $\$/kWh$ for the acquisition of the TES [5] and an OM cost in the range of 10.5 and 12.6 $\$/MWh$[25], with the average of 11.55 $\$/MWh$ being the value implemented in the present work.

3.3. ORC Module Costs

According to information obtained from the manufacturer (Michael Welch 2018, personal communication, 18 June 2018), the acquisition price may be assumed as 1000 $\$/kW$, with a maintenance cost of 2.50 $\$/MWh$.

3.4. LCOE Calculation

The LCOE was calculated using equation 18 from [19] with an insurance cost added to the OM costs of 0.5% of the cost of capital as in:

$$LCOE = \frac{fcr \cdot C_{invest} + C_{OM} + C_{fuel}}{E_{net}} \tag{18}$$

The annuity factor is calculated with equation 19 from [26]:

$$fcr = (\frac{1-(1+r)^{-n}}{r})^{-1} \tag{19}$$

4. Annual Simulation

Once the solar field model was implemented in Engineering Equation Solver (EES) and the TES and Economic Analysis in a spreadsheet, it was possible to predict what the results would look like after a year-long operation of the power plant. Figure 2 depicts the energy flows beginning with the incident radiation until the electricity produced by the power plant and the thermal energy stored on a sample day. At the first sunlight hour of the day, the radiation is still not enough to justify the startup of the system until around 7 am, when the incident

radiation reaches values close to 15 MW, so the HTF starts circulating and the ORC module starts its power production until it reaches base load operation with a 1 MW gross output. Between 7 and 8 am, the Thermal Power coming from the solar field reaches values superior to the one demanded by the power block at nominal operation, hence providing the overbalance to the TES, which accumulates the thermal power until around 4 pm, when it starts providing energy to keep the ORC module in baseload until 11 pm. At that point, the electrical output starts decaying until 1 am, when the power block is shut down. From the graph, we can see that the power plant functions at base load during the highest demand hours, which are usually between 10 am and 8 pm, according to [19]. The operation day of the graph is an example of a clear sky day, where the TES was needed only to keep production during the darkest hours and not to secure stable generation during the daytime. To illustrate the present discussion, Figure 3 shows the Sankey diagram of the same day as the previous plot (Figure 2), but specifically for the operation at 12 pm. It displays the energy flows throughout the system for an instant of high solar incidence level, when a great share of the thermal energy harvested is stored in the molten salt tanks. From the total direct incident solar power, 54.8% is harvested by the solar field, and 45.2% is lost to the ambient because of a variety of reasons, already highlighted in Section 2.2. For the analysed instant, we have a large overproduction of heat by the collectors, which implicates more than 60% of the produced heat being stored in the TES while only 39.8% is destined for the power block for power production. The ORC module selected has a 24.7% gross efficiency, and 75.3% of the heat supplied in the evaporator is rejected in the condenser.

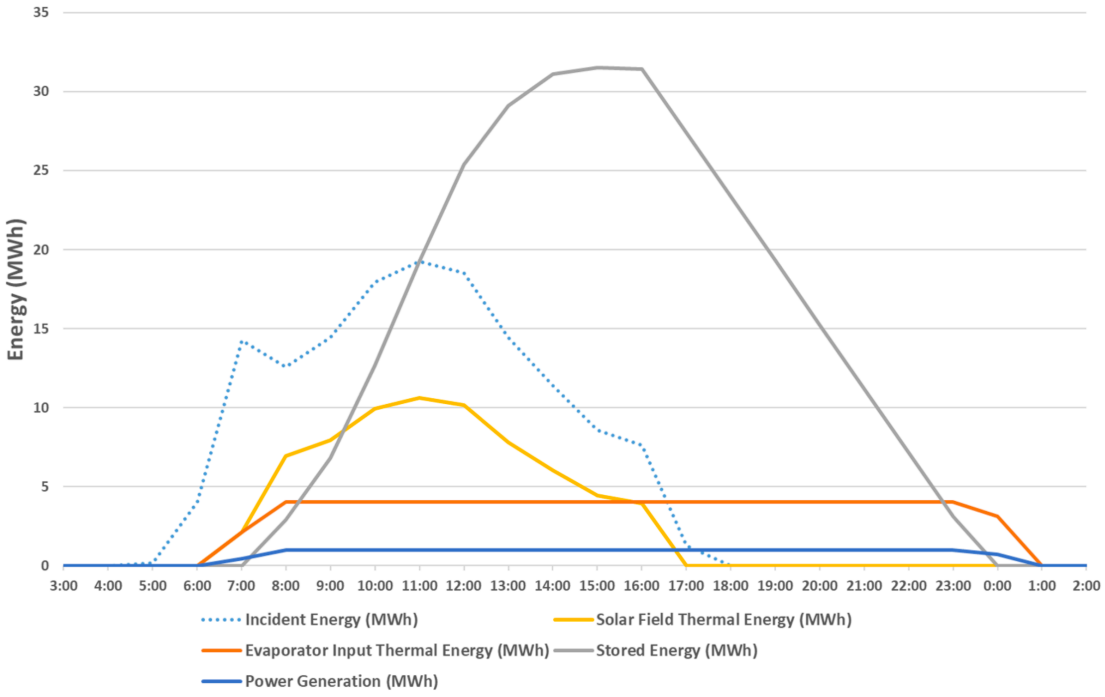

Figure 2. Energy flows in the power plant from incident radiation to generated power for a sample day.

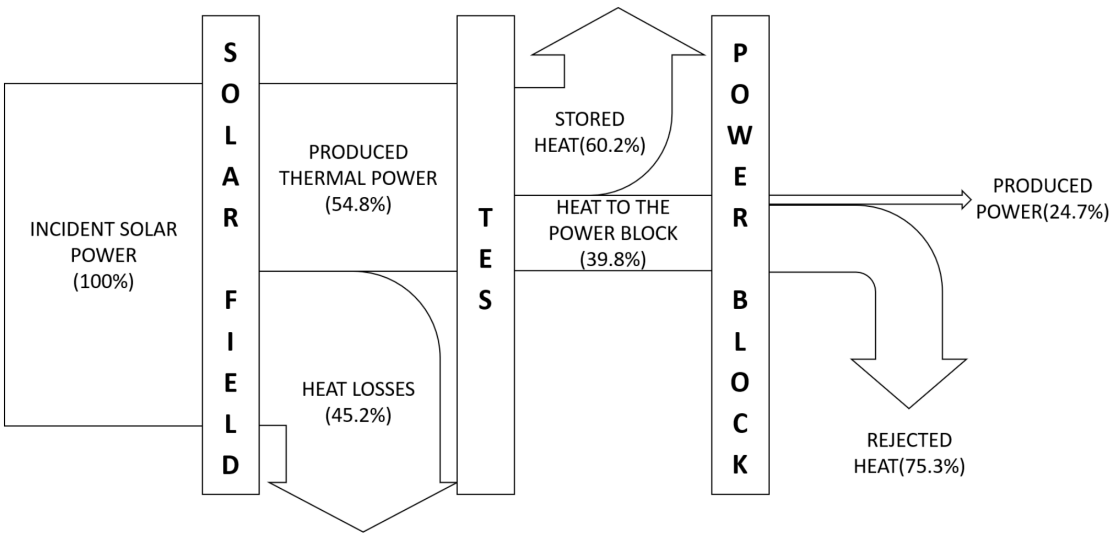

Figure 3. Sankey diagram for energy flow for a sample day at 12 pm.

In this section, the behaviour of the power plant on an hourly and daily scale was displayed and analysed in order to provide a better understanding of the energy flows through the systems that compose the power plant

doi.org/10.32388/NKKKOI

and the efficiencies associated with the process. In the next sections, the results of a year-round operation will be discussed in terms of technical and economic aspects, and conclusions will be drawn regarding the relevant resulting data.

5. Results and Discussion

Based on what was presented, Figure 4 displays the effect of the TES capacity on the LCOE for the different solar field-sized configurations. It's possible to observe that the case where an SM of 2.85 has the curve that reaches the lowest points in comparison to the other four curves, whose points are in the direction that it is the optimum configuration from the ones considered.

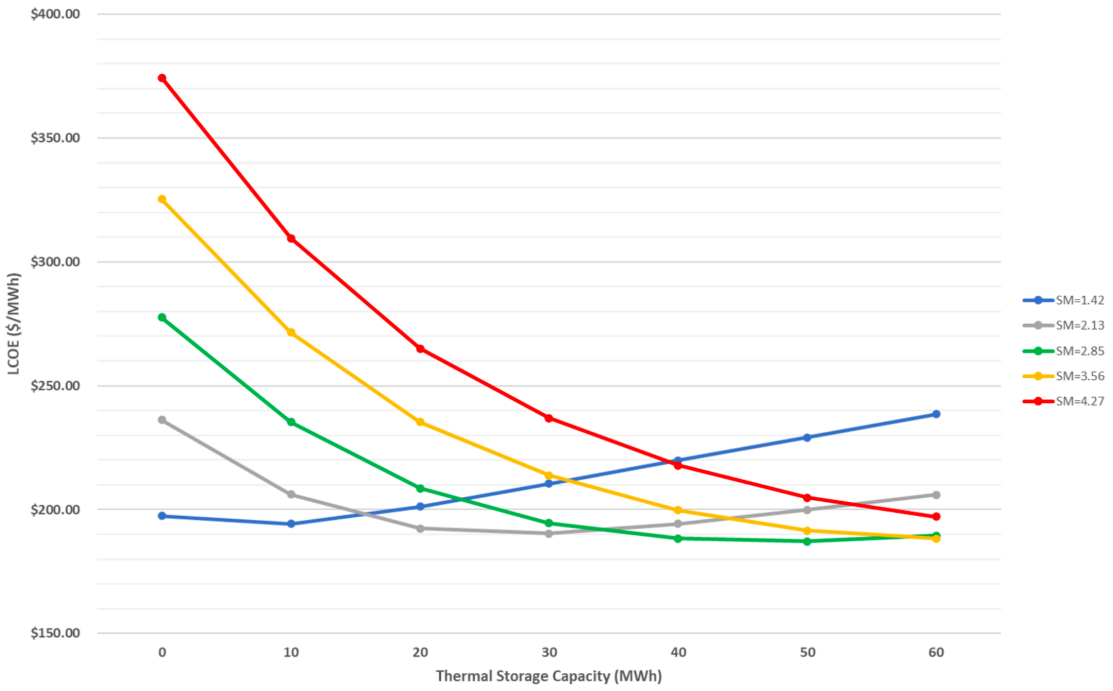

Figure 4. LCOE variation according to installed TES capacity for five different solar multiples.

After a careful analysis, it is possible to determine the optimum TES capacity for each solar field size and utilize them to summarize the results for each solar multiple and compare the values for the configurations with and without TES. Those resulted in the configurations shown in tables 6 and 7, where the main technical and financial results for each configuration are displayed.

doi.org/10.32388/NKKKOI

With TES					
Configuration	**Solar Multiple [-])**	**Net Power Generated [MWh]**	**Power Plant Efficiency [-]**	**CO2 Avoided [ton]**	**People attended**
50/8MWh	1.42	2353.59	11.81%	952.14	1676
75/27MWh	2.13	3556.26	11.90%	1438.69	2533
100/48MWh	2.85	4815.50	12.08%	1948.11	3430
125/59MWh	3.56	5836.80	11.72%	2361.28	4157
150/63MWh	4.27	6488.05	10.85%	2624.74	4621
Without TES					
Configuration	**Solar Multiple [-]**	**Net Power Generated [MWh]**	**Power Plant Efficiency [-]**	**Avoided CO2 [ton]**	**People Attended**
50	1.42	2079.25	10.44%	841.16	1481
75	2.13	2524.23	8.09%	978.58	1723
100	2.85	2704.67	6.61%	1065.77	1876
125	3.56	2812.83	5.50%	1108.37	1951
150	4.27	2882.63	4.70%	1135.86	2000

Table 6. Technical results for the different configurations considered after one year of operation.

With TES				
Configuration	**Solar Multiple [-]**	**Initial investment [US$]**	**Annual maintenance cost [US$]**	**LCOE [$/MWh]**
50/8MWh	1.42	4,397,260.00	80,000.24	193.93
75/27MWh	2.13	6,489,190.00	120,403.56	190.08
100/48MWh	2.85	8,633,560.00	161,445.97	186.98
125/59MWh	3.56	10,515,730.00	199,212.54	188.33
150/63MWh	4.27	12,214,360.00	231,719.22	196.85
Without TES				
Configuration	**Solar Multiple [-]**	**Initial investment [US$]**	**Annual maintenance cost [US$]**	**LCOE [$/MWh]**
50	1.42	4,187,500.00	52,084.14	197.47
75	2.13	5,781,250.00	76,297.00	236.20
100	2.85	7,375,000.00	100,014.73	277.57
125	3.56	8,968,750.00	123,545.12	325.28
150	4.27	10,562,500.00	146,976.04	374.33

Table 7. Financial results for the different considered configurations.

According to the results shown, the most viable configuration is the one with an SM of 2.85 and 48 MWh of TES capacity, since it presented the lowest LCOE with the highest efficiency. This result can be understood as, for the specific ORC module chosen for the specific site analysed, the optimum configuration is the one displaying the best financial results from all the considered configurations. With the 1MW ORC module chosen, any extra investment to increase the solar field or TES sizes would, of course, result in an increase in energy production but also an even higher cost addition, resulting in more expensive electricity for that power plant. Figure 5 shows the net energy generated per month and the monthly average. It is possible to see that the first semester months are below the average. This can be explained by the fact that the region typically goes through a high precipitation season during this period, while the second half of the year is marked by dry weather, fewer clouds, and therefore higher power generation. The relation between the generation in April, the worst month, and September, the best month in energy generated quantity, is 0.46. That proportion shows that the variation throughout the year is not too expressive when compared to the numbers in the order of 0.3 found by other authors [3]. This points in the direction of showing the location as a good one for such a type of project, since it would demand less generation compensation from the system operator in the months with less generation.

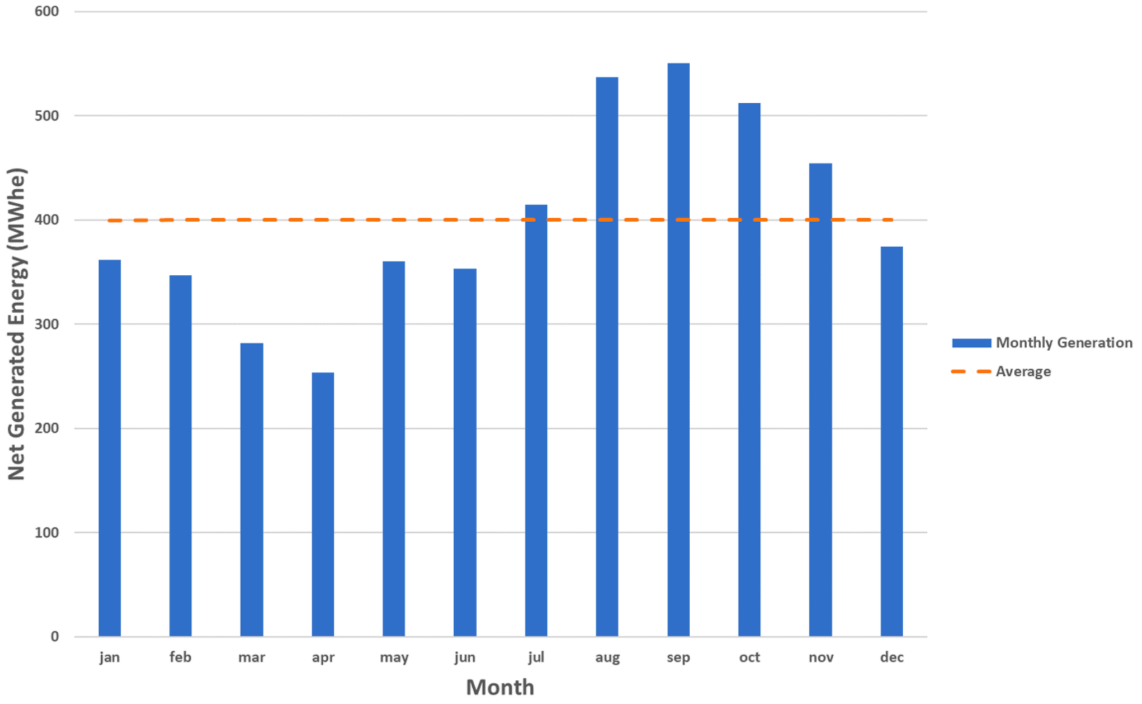

Figure 5. Monthly power generation for the optimum configuration.

Figure 6 displays the capital cost of the three main systems of the selected power plant: the solar field, TES, and power block, as well as their sum. It is noticeable that the solar field accounts for the biggest share of the whole investment, reaching about 74% of the total capital cost, followed by the TES, and then the ORC module, with a slightly smaller number. That is a result that is in accordance with the typical numbers displayed by CSP power plants as stated by [5]. Figure 7 displays a similar distribution but regarding the O&M costs of those systems. Again, the solar field accounts for the biggest share of around 58%, but what is worth highlighting is the drastically small O&M cost of the ORC module compared to the other two systems, with a share of only 8% of the total annual cost. In the present section, it was possible to analyse the technical and economic aspects of each system of the power plant and of the power plant as a whole and compare different possible configurations for the project. Furthermore, the seasonality of the chosen region was analysed in order to determine the variation of the produced energy along the months.

doi.org/10.32388/NKKKOI

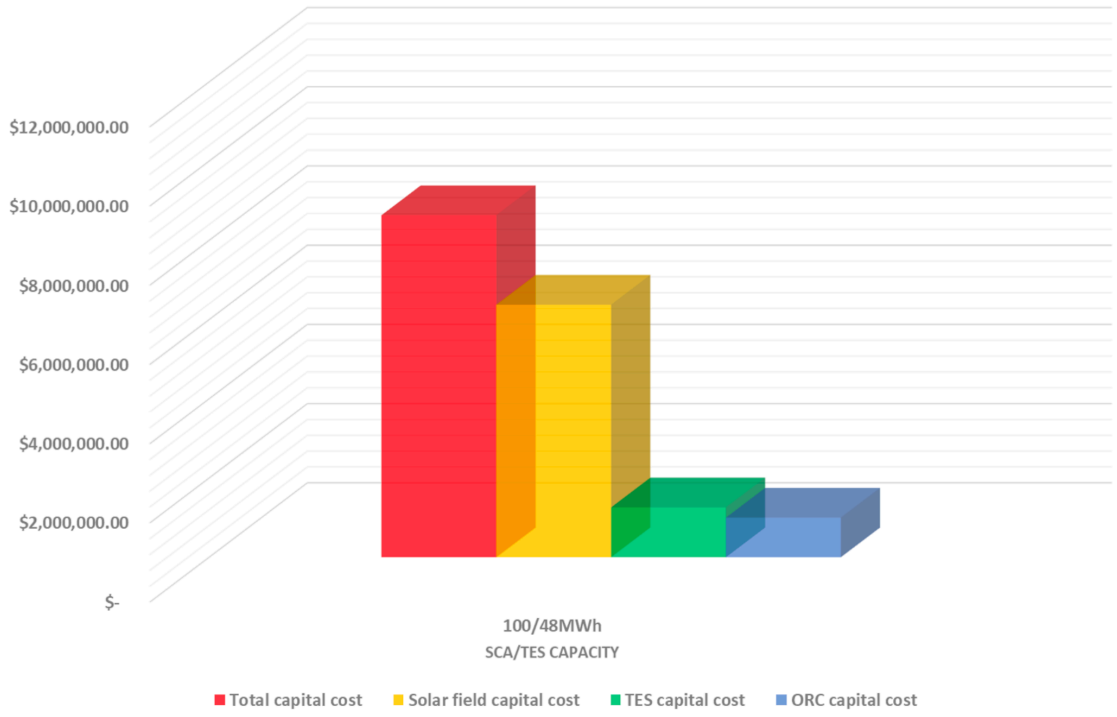

Figure 6. Capital costs of the power plant for the optimum configuration.

doi.org/10.32388/NKKKOI

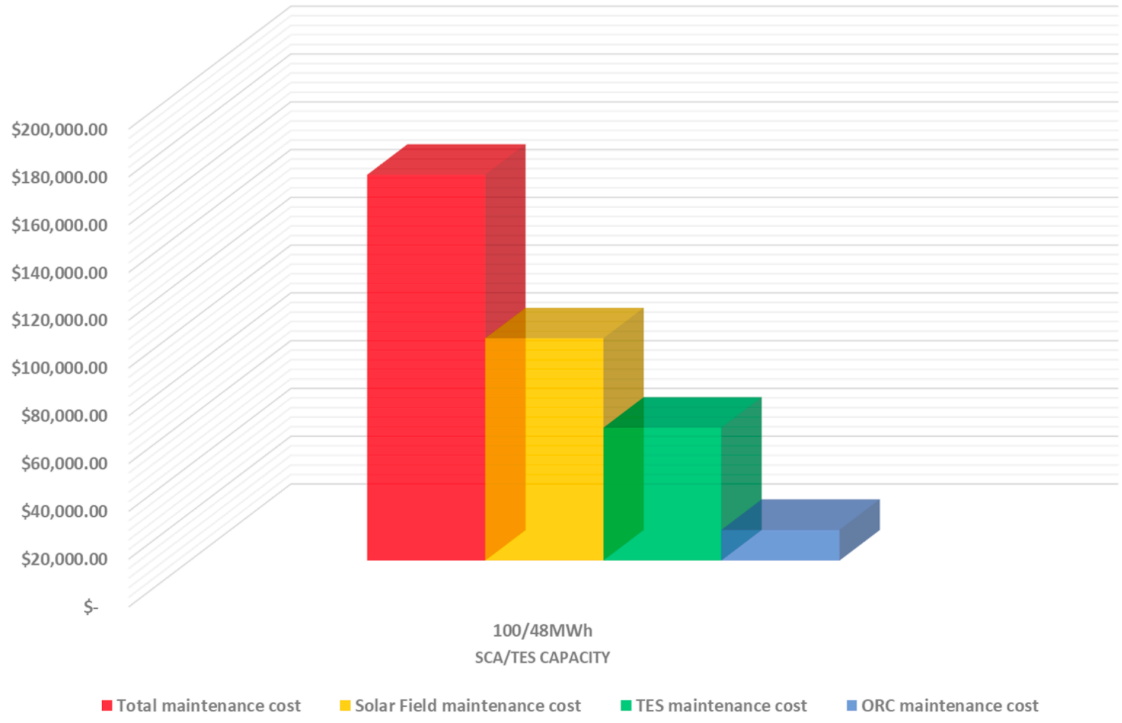

Figure 7. O&M costs of the power plant for the optimum configuration.

6. Conclusion

The stand-alone 1MW Organic Rankine Cycle (ORC) CSP power plant was simulated with the local weather data for 5 different solar multiple (SM) values: 1.42, 2.13, 2.85, 3.56, 4.27, and with different thermal energy storage (TES) capacities, starting from rule storage capacity up to values as high as 60 MWh. The levelized cost of electricity (LCOE) of each configuration was calculated, and it was possible to determine the optimum configuration from the considered ones as 100 collectors and 48 MWh of TES capacity, with an LCOE of 186.98 USD/MWh. This value is considerably high when compared to bid tariffs of around 60 USD/MWh reported in Chile and Australia [2], the LCOE of the order of 110 USD/MWh achieved [1] for a hybrid CSP/Biomass power plant in the northeastern region of Brazil, and the 87.4 USD/MWh obtained for Morocco [13]. Nevertheless, as the capital and O&M costs of the power plant are analysed, it is possible to highlight the small contribution of the ORC module in those quantities, 12% and 8% respectively, and the large majority presented by the solar field, 73.8% and 58% respectively. Given that, the paper points out the possibility of optimization mainly in the solar field, possibly by the implementation of a more recent model of collector. Another important remark is the advantage the TES brings to the feasibility of the project, since the lowest LCOE achieved without such a system was 197.47 USD/MWh. Regarding the chosen region, it presents itself as a good option for such a project, not

only due to the high DNI and average temperature levels but also because the monthly generated power variations were low, which shows a fair stability of the power plant throughout the year, making it more attractive to the system operator.

Acknowledgments

This study was financed in part by the Coordenacao de Aperfeicoamento de Pessoal de Nivel Superior - Brasil (CAPES) - Finance Code 001 and was accomplished with the support of the Conselho Nacional de Desenvolvimento Cientifico e Tecnologico - Brasil (CNPq) - Grant No. 305456/2019-9, both Brazilian governmental agencies.

References

1. a, b, c, d *(2015). Hybrid concentrated solar power (CSP)–biomass plants in a semiarid region: A strategy for CSP deployment in Brazil. Energy Policy, 86, 57–72. https://doi.org/10.1016/j.enpol.2015.06.028*
2. a, b, c *Secretariat, P. R. (2018). Renewables 2018 Global Status Report. Tech. rep.*
3. a, b *(2012). Comparison of different solar plants based on parabolic trough technology. Solar Energy, 86(5), 1208–1221. https://doi.org/10.1016/j.solener.2012.01.014*
4. a, b, c *IRENA. (2012). Concentrating solar power, Renewable Energy Technologies: Cost Analysis Series. Tech. rep.*
5. a, b, c *(2017). Thermal energy storage systems for concentrated solar power plants. Renewable and Sustainable Energy Reviews, 79, 82–100. https://doi.org/10.1016/j.rser.2017.03.139*
6. a, b, c *Duffie, J. & Beckman, W. A. (2006). Solar Engineering of Thermal Processes (3rd ed.). Wiley.*
7. ^ *(2020). Perspective of concentrating solar power. Energy, 198, 117373. https://doi.org/10.1016/j.energy.2020.117373*
8. ^ *(2014). Operation of a fully renewable electric energy system with csp plants. Applied Energy, 119, 417–430. https://doi.org/10.1016/j.apenergy.2014.01.014*
9. ^ *(2019). Is concentrated solar power (CSP) a feasible option for sub-Saharan Africa?: Investigating the techno-economic feasibility of CSP in Tanzania. Renewable Energy, 135, 1224–1240. https://doi.org/10.1016/j.renene.2018.09.065*
10. a, b *(2018). Economic justification of concentrating solar power in high renewable energy penetrated power systems. Applied Energy, 222, 649–661. https://doi.org/10.1016/j.apenergy.2018.03.161*
11. a, b, c *ONS. (2018). Curva de carga horária. http://ons.org.br/Paginas/resultados-da-operacao/historico-da-operacao/curva-carga-horaria.aspx*
12. ^ *de Lima, E. B. P. F. R. M. A. R. G. R. S. C. F. J. L., Ruether, R., de Abreu, S. L., Tiepolo, G. M., Pereira, S. V., & de Souza, J. G. (2017). Atlas brasileiro de energia solar. Tech. rep.*

13. ^a ^b *(2021). Determination of design parameters to minimize LCOE, for a 1 MWe CSP plant in different sites. Renewable Energy, 169, 1013–1025. https://doi.org/10.1016/j.renene.2021.01.060*
14. ^ *(2015). Electrical production of a small size concentrated solar power plant with compound parabolic collectors. Renewable Energy, 83, 1110–1118. https://doi.org/10.1016/j.renene.2015.03.033*
15. ^ *Barua, A., Chakraborty, S., Paul, D., & Das, P. (2015). Analysis of concentrated solar power technologies' feasibility, selection and promotional strategy for Bangladesh. Journal of Mechanical Engineering, 44, 112. https://doi.org/10.3329/jme.v44i2.21435*
16. ^ *NREL. (2017). Meteorology: typical meteorological year data for selected stations in Brazil from NREL. http://en.openei.org/datasets/dataset/meteorology-typical-meteorological-year-data-for-selected-stations-in-brazil-from-nrel*
17. ^a ^b ^c ^d ^e ^f ^g ^h ^i ^j ^k *Patnode, A. M. (2006). Simulation and Performance Evaluation of Parabolic Trough Solar Power Plants. Master's thesis, University of Wisconsin-Madison.*
18. ^a ^b ^c *Turboden. (2016). Organic Rankine Cycle Technology, Turboden 12 HRS - 1MW Datasheet. http://www.turboden.eu*
19. ^a ^b ^c *(2009). Solar multiple optimization for a solar-only thermal power plant, using oil as heat transfer fluid in the parabolic trough collectors. Solar Energy, 83(12), 2165–2176. https://doi.org/10.1016/j.solener.2009.08.010*
20. ^ *Winter, S. R. L. V.-H. L. L. E., & C.-J. (1991). Solar Power Plants (1st ed.). Springer-Verlag Berlin Heidelberg.*
21. ^ *Forristall, R. (2003). Heat Transfer Analysis and Modeling of a Parabolic Trough Solar Receiver Implemented in Engineering Equation Solver. Tech. rep.*
22. ^ *(2018). Hybridizing a geothermal power plant with concentrating solar power and thermal storage to increase power generation and dispatchability. Applied Energy, 228, 1837–1852. https://doi.org/10.1016/j.apenergy.2018.07.064*
23. ^ *(2017). Maintenance of a small-scale parabolic trough concentrating solar power plant in Louisiana. International Journal of Sustainable and Green Energy, 6, 104–111. https://doi.org/10.11648/j.ijrse.20170606.12*
24. ^ *Glatzmaier, G. (2011). Developing a Cost Model and Methodology to Estimate Capital Costs for Thermal Energy Storage. Tech. rep.*
25. ^ *(2017). Review of commercial thermal energy storage in concentrated solar power plants: Steam vs. molten salts. Renewable and Sustainable Energy Reviews, 80, 133–148. https://doi.org/10.1016/j.rser.2017.05.084*
26. ^ *Kagan, J. (2020). Present value of an annuity. https://www.investopedia.com/terms/p/present-value-annuity.asp*

Declarations

Funding: This study was financed in part by the Coordenação de Aperfeiçoamento de Pessoal de Nível Superior - Brasil (CAPES) - Finance Code 001 and accomplished with the support of the Conselho Nacional de Desenvolvimento Científico e Tecnológico - Brasil (CNPq) - Grant No. 305456/2019-9, both Brazilian governmental agencies.

Potential competing interests: No potential competing interests to declare.